Organic monolayers modified by vacuum ultraviolet irradiation for solution-processed organic thin-film transistors

Inoue, Satoshi
Hattori, Yoshiaki
Kitamura, Masatoshi

(Citation)
Japanese Journal of Applied Physics,61(SE):SE1012

(Issue Date)
2022-06-01

(Resource Type)
journal article

(Version)
Accepted Manuscript

Organic monolayers modified by vacuum ultraviolet irradiation for solution-processed organic thin-film transistors

Satoshi Inoue, Yoshiaki Hattori[*]*, and Masatoshi Kitamura*[**]

Department of Electrical and Electronic Engineering, Kobe University, 1-1, Rokkodai-cho, Nada-ku, Kobe, 657-8501, Japan

Corresponding Author

Email: [*]hattori@eedept.kobe-u.ac.jp, [**]kitamura@eedept.kobe-u.ac.jp

Keywords:

OTFTs, vacuum ultraviolet, modification, trap sites, C_8-BTBT

ABSTRACT:

A trimethylsilyl-monolayer modified by vacuum ultraviolet (VUV) light has been investigated for use in solution-processed organic thin-film transistors (OTFTs). The VUV irradiation changed a hydrophobic trimethylsilyl-monolayer formed from hexamethyldisilazane vapor into a hydrophilic surface suitable for solution processing. The treated surface was examined via water contact angle measurement and X-ray photoelectron spectroscopy. An appropriate irradiation of VUV light enabled the formation of a dioctyl[1]benzothieno[3,2-b][1]benzothiophene (C_8-BTBT) film on a modified monolayer by spin-coating. Consequently, the C_8-BTBT-based OTFT with a monolayer modified for an optimal VUV irradiation time exhibited a field-effect mobility up to 4.76 $cm^2 V^{-1} s^{-1}$. The partial monolayer modification with VUV can be adapted to a variety of solution-processes and organic semiconductors for prospective printed electronics.

1. Introduction

Organic thin-film transistors (OTFTs) fabricated by solution-processes have attracted vast attention because of their cost-effectivity, scalability, and compatibility with flexible substrates. Soluble organic semiconductor materials for high-performance OTFTs have been developed in the recent decade. The field-effect mobility in OTFTs fabricated by solution-process has exceeded 10 $cm^2\ V^{-1}\ s^{-1}$.[1–3] The use of a high mobility material is a necessary condition, not a sufficient condition to achieve a high-performance OTFT. The following properties in OTFTs influence the transistor performance: the contact resistance with the electrodes, crystallinity of the organic thin-film, gate dielectric properties, and device structure. Thus, it is important to develop the fabrication processes appropriate for latest soluble organic semiconductors. For OTFTs with a bottom gate structure, the gate dielectric should have a surface suitable for coating an organic layer in the solution-process and for optimal electrical properties. Since charge carriers are transported in the organic channel layer a few nanometers away from the interface between the organic layer and gate dielectric,[4] carrier trap sites on the gate dielectric surface significantly affect the device performance. Thus, the control of the gate dielectric surface is a critical issue in obtaining high-performance OTFTs.

For OTFTs, trap sites at the dielectric-organic layer interface decrease the carrier mobility, causing hysteresis in the electrical characteristics.[5, 6] Hydroxyl groups (−OH) on the dielectric surface possibly serve as trap sites in the OTFTs, leading to a hydrophilic surface. It has been experimentally confirmed that a substrate with a hydrophobic gate dielectric surface with low surface free energy suppresses the trap sites and improves the transistor performance.[7–9] Thus, dielectric materials without −OH groups are used as a gate dielectric in OTFTs.[6, 10] Another way to reduce trap sites is the use of a gate dielectric layer modified with an organic monolayer. In the

technique, a hydrophobic methyl-terminated monolayer, formed from octadecyltrimethoxysilane (OTS),[11, 12] hexamethyldisilazane (HMDS),[13, 14] or octadecylphosphonic acid (ODPA),[15, 16] is widely employed to decrease the surface free energy of a substrate. For the fabrication of OTFTs with a bottom gate structure, the use of gate dielectric with a methyl-terminated monolayer is suitable for an organic layer prepared by vacuum deposition, not suitable for that via the solution-process. This is because the hydrophobic surface makes the coating with an organic layer via solution-process difficult. In general, the surface wettability of a solution is required for the coating processes, such as spin-coating,[17] dip-coating,[18] edge-casting,[19] drop-casting,[20] and inkjet-printing.[21] A method to ensure the wettability for solution-processes is the use of a phenyl-terminated monolayer formed from phenyltrichlorosilane or phenyltrimethoxysilane,[22] which induces higher surface free energy as compared to a methyl-terminated monolayer.[23]

For the deposition of organic films by printing, a gate dielectric covered with two types of monolayers has been used to obtain partially different wettability, realized by the patterning of the monolayer.[24, 25] In the patterning technique, irradiating vacuum ultraviolet (VUV) light with a wavelength less than 200 nm through a shadow mask photochemically dissociates the hydrophobic monolayer in the irradiated area, formed from OTS,[26–28] fluoroalkylsilane,[29] HMDS,[22] or ODPA.[30] Then, a different monolayer is formed on the eliminated area, decreasing the trap sites on the surface.[22, 28–30]

The photochemical reaction of an alkyl-monolayer with active oxygen species generated from oxygen molecules in air by VUV irradiation has been widely studied.[31–33] At the first stage of the reaction, the active oxygen specie oxidizes the hydrophobic methyl-terminated group ($-CH_3$) and generates hydrophilic oxygenated carbon components, such as primary alcohol group ($-CH_2OH$) with C-O bond, aldehyde group ($-CHO$) with C=O, and carboxyl group ($-COOH$)

with C-O and C=O bonds, which increase the surface energy. Additionally, the long irradiation time causes decomposition of alkyl chain in the monolayer. The successive reaction shortens the alkyl chains until it completely dissociates the alkyl groups.

For VUV irradiation at the surface with a monolayer, the surface energy increases with an increase in the irradiation time.[32, 34, 35] Thus, adjusting the irradiation time enables the tuning of the monolayer surface energy. Prisawong *et al.* have investigated the influence of morphology of organic semiconductor films deposited by vacuum-process on the characteristics of OTFTs with an ODPA-treated AlO_x gate dielectric modified by VUV with different irradiation times.[36] In the study, the carrier mobility of the OTFT decreased with an increase in the VUV irradiation time. They have explained that the decrease is attributed to the difference in the organic film morphology at the initial stage of growth, which depends on the surface energy. If a hydrophilic VUV-treated monolayer is applied for the solution-process, different insights on the dependency of VUV irradiation time might be confirmed. This is because the growth mechanism of solution-process is different from that of vacuum-process. The short VUV irradiation time adjusted for the solution-process is expected to form the hydrophilic surface with low density of trap sites. Although we have proposed the use of VUV-irradiated monolayer for solution-process,[37] the relationship between the hydrophilic surfaces and OTFT characteristics has not been studied in detail.

In this study, we investigate the characteristics of solution-processed OTFTs having an organic channel layer deposited on a trimethylsilyl-monolayer modified by ultraviolet (UV) light. A soluble organic semiconductor, 2,7-Dioctyl[1]benzothieno[3,2-b][1]benzothiophene (C_8-BTBT), was used as a channel material. The trimethylsilyl-monolayer was formed on the SiO_2 surface using HMDS vapor and modified by UV light with wavelengths of 185 and 254 nm emitted from an ozone lamp for different irradiation times. The effect of the irradiation is evaluated by

water contact angle measurement and coating of C_8-BTBT film. We expect that the irradiation of VUV light with a wavelength of 185 nm generates hydrophilic oxygenated carbon components. In addition, the effect of the irradiation on the characteristics of OTFTs with a trimethylsilyl-monolayer may be observed more clearly as compared to that for a long-alkyl-monolayer. Then, electrical properties of OTFTs with a C_8-BTBT layer formed by spin-coating are shown. The influence of UV irradiation on the transistor characteristics is examined. Furthermore, the effect of UV irradiation on a trimethylsilyl-monolayer is discussed based on results of the surface measurement via X-ray photoelectron spectroscopy (XPS).

2. Experimental methods

OTFTs examined in this study were fabricated according to the fabrication process shown in Figs. 1(a)–1(f). Highly doped n-type Si substrates with a 94 nm-thick SiO_2 layer were used. The thickness of the SiO_2 layer serving as a gate dielectric corresponds to a capacitance per unit area (C_{ox}) of 36.6 nF/cm^2. The substrate was cleaned in organic solvents by ultrasonication, and later irradiated with UV light from an ozone lamp (GL10ZH, Sankyo) in air for 30 min. In general, UV light with a wavelength of around 200 nm generates ozone and reactive oxygen species, which decompose organic contaminants on a substrate surface. For the OTFT fabrication, the substrate was placed 45 mm away from the ozone lamp. The characteristics of the ozone lamp are mentioned in Section 3. Immediately after UV irradiation, the substrate was exposed to HMDS vapor at 120°C for 30 min to form trimethylsilyl-monolayer. Then, the substrate was UV irradiated under the same conditions to obtain a hydrophilic surface for solution-process. The second UV irradiation time, t_{uv}, was set to 0 and 60 min. An organic layer of C_8-BTBT on the substrate was prepared via a two-step spin-coating of 500 rpm for 5 s and 2000 rpm for 30 s, subsequently using a chlorobenzene solution with 0.5 wt% concentration. The C_8-BTBT film had a thickness of about 15 nm, which

was measured with an atomic force microscope in tapping mode. A 40 nm-thick Au layer was deposited by vacuum evaporation through a shadow mask to form source/drain electrodes. The channel length (L) and width (W) are 200 μm and 1400 μm, respectively. To isolate the OTFTs, an area of C_8-BTBT layer outside of a source/drain electrode pair was scraped off with a fine needle. A photograph of an isolated OTFT is shown in Fig. 1(g). The electrical characteristics of OTFTs were measured with a semiconductor parameter analyzer (B1500, Agilent) in a dry nitrogen-filled glove box at room temperature. The XPS spectra of substrate surfaces with a monolayer were measured by a PHI-X-tool (ULVAC-PHI) with a monochromatized Al Ka X-ray source.

3. Preparation of organic thin films

To clarify the possibility of photochemical reaction by UV light used in this study, the spatial distribution of the light intensity around the UV lamp was investigated. The UV light irradiated from the ozone lamp has two main peaks at 185 nm and 254 nm. The light intensities at corresponding wavelengths were measured using the illumination photometers; UIT-150-A with VUV-S172, Ushio and UV-MO2 with UV-25, ORC, respectively. The detectors of VUV-S172 and UV-25 were calibrated at 172 nm and 254 nm, respectively. The VUV-S172 detector was also sensitive to light of a wavelength of 185 nm. Figure 2 (a) shows the distribution of the light intensity measured using the illumination photometer. The horizontal axis represents the distance of the detector from the cylindrical axis of the ozone lamp, x, as shown in the schematic on the left. The solid red and black lines show the light intensities measured by detectors of VUV-S172 for 185 nm and UV-25 for 254 nm, respectively. For both wavelengths, the intensity monotonically decreases with an increase in x. The intensity for 185 nm is roughly four times as high as that for 254 nm. The solid orange line shows the sum of the intensities for 185 and 254 nm. To verify the

measured values, the total intensity is compared to that estimated from the power consumption of the lamp, P (= 10 W), using $P/(2\pi L_{uv}x)$ where L_{uv} (300 mm) is the length of the lamp. The solid blue line in Fig. 2(a) shows the estimated intensity, which is close to the total intensity. The comparison implies that the measured intensities are not irrelevant. The intensities of 185 and 254 nm at 45 mm where the substrates are placed in the fabrication of OTFTs are 7.3 and 2.6 mW/cm^2, respectively. In general, the light of 185 nm rather than that of 254 nm is effective for photochemical reaction. The intensity of 7.3 mW/cm^2 at 185 nm indicates that 68 photons are incident on the area of 1 nm^2 per 1 s. It seems that the number of photons satisfies a necessary condition for a photochemical reaction to occur in about 1 to 10 min.

Figure 2(b) shows the water contact angle on a substrate with a trimethylsilyl-monolayer irradiated to UV light for t_{uv}. The substrate with a trimethylsilyl-monolayer without the second UV irradiation exhibited a hydrophobic surface with a contact angle of about 90°. The contact angle gradually decreased with an increase in t_{uv} and almost reached zero at t_{uv} = 15 min. The origin of the change will be discussed later in the discussion section.

Figure 2(c) shows the photographs of the organic thin-film deposited by spin-coating with a different second UV irradiation time (t_{uv}). The blue part of the substrate is the area covered with the C_8-BTBT film. The left most photograph shows the substrate without monolayer for which the spin-coting was performed immediately after the first UV irradiation. In general, the UV irradiation decomposed the surface contaminants and formed hydrophilic silanol groups (≡SiOH) on the SiO_2 surface. In actual, the water contact angle was almost 0° (not shown), indicating that the surface had a high surface energy. The surface condition allows the formation of the organic thin-film over the entire surface by spin-coating, as seen in the photograph in Fig. 2(c). Conversely, a hydrophobic monolayer prevented organic thin-film formation by solution-process. The UV light

irradiation on the substrate with a trimethylsilyl-monolayer was effective in forming organic thin-film by solution-process. The area covered with the C_8-BTBT film increased with an increase in t_{uv}, as seen in Fig. 2(c). For t_{uv} = 10–12 min, the substrate was partially covered with a C_8-BTBT film, while for $t_{uv} \geq 15$ min, the substrate was fully covered with the C_8-BTBT film. This suggests that the UV irradiation for $t_{uv} \geq 15$ min enabled the formation of an organic thin-film on the entire surface.

The crystallinity of a C_8-BTBT film formed by spin-coating was evaluated via an optical microscope. Figure 3 shows the optical microscope images of a C_8-BTBT film for the second UV irradiation of t_{uv} = 10 min. Figure 3(a) is the bright-field microscopy image. Figures 3(b) and 3(c) show the polarized light microscopy images of an area different from that in Fig. 3(a). Figures 3(b) and 3(c) are the photographs of the same area. The two yellow arrows in the images with "P" and "A" indicate the transmission axes of the polarizer and analyzer, respectively. The angle between the two transmission axes was intentionally rotated by about 5° from 90° to enhance the contrast related to the crystal orientation of an organic thin-film.[38] Similar colors in a picture indicated domains with the same crystal axis direction, although the thickness of an organic film also influenced the color. The area surrounded by a white dashed line in Fig. 3(b), which is the same area as that in Fig. 3(c), indicates a typical domain. The C_8-BTBT film is composed of grains of about 10 μm. Similar crystallinities were also observed in the C_8-BTBT films for other t_{uv}.

4. Transistor characteristics

Figures 4(a)–4(c) shows the drain current (I_d) versus gate voltage (V_g) characteristics of the OTFTs in the saturation regime at a drain voltage (V_d) of −20 V. Also, the gate current (I_g) is shown in Figs. 4(a)–4(c). Figure 4(a) shows the characteristics for an OTFT without HMDS treatment, the C_8-BTBT layer of which corresponds to the leftmost picture in Fig. 2(c). Figures 4(b) and 4(c)

are the characteristics for t_{uv} = 12 and 60 min, respectively. The gate leakage current of OTFTs was less than 0.1 nA, as seen in Figs. 4(a)–(c). Figure 4(d) shows I_d versus V_d characteristics at different V_g of an OTFT for t_{uv} = 12 min. These transfer and output curves exhibited the characteristics of a typical *p*-channel OTFTs. The field-effect mobilities in the saturation regime (μ_{sat}) and threshold voltage (V_{th}) of the OTFT were estimated by using the following equation extracted from conventional gradual channel approximation:

$$I_d = \frac{1}{2}\frac{W}{L}\mu_{sat}C_{ox}\left(V_g - V_{th}\right)^2. \quad (1)$$

For Figs. 4(a) and (c), the hysteresis clearly appeared in the forward (from 2 V to −20 V) and reverse (from −20 V to 2 V) sweeps of V_g in the transfer curve. For Fig. 4(b), the transfer curve in the forward sweep is close to that in the reverse sweep. To quantify the hysteresis, we defined threshold voltage difference as $\Delta V_{th} = V_{thr} - V_{thf}$ where V_{thr} and V_{thf} are V_{th} estimated from transfer curves in the forward and reverse sweeps, respectively. The electrical properties of typical OTFTs for different t_{uv} examined in this study are summarized in Table 1, including μ_{sat}, V_{thf}, V_{thr}, ΔV_{th}, and the current on/off ratio.

Figures 5(a) and 5(b) show the μ_{sat} and ΔV_{th} values estimated from the transfer curves of OTFTs for t_{uv}, respectively. The closed circles indicate an average value. The upper and lower limits of the error bar show the largest and smallest values for t_{uv}. The number of OTFTs for t_{uv} = 10−15 min was seven, and that for the other t_{uv} was two. We focused on the characteristics of OTFT for t_{uv} = 10−15 min. A large hysteresis was observed in OTFTs with low μ_{sat}. For the OTFT without a monolayer, a large hysteresis appeared in the transfer curve as ΔV_{th} = −6.36 V. As seen in Fig. 5(b), the formation of a monolayer suppressed the hysteresis even if the surface with a monolayer was irradiated with UV light for a long time. Conversely, the field-effect mobility (μ_{sat}) seems to be more sensitive to the irradiation time t_{uv}. There was an optimal t_{uv} for μ_{sat}, as seen in

Fig. 5(a). For the OTFT with t_{uv} = 12 min, the hysteresis was the smallest and the average μ_{sat} was the highest at 4.10 $cm^2\ V^{-1}\ s^{-1}$. The OTFT for t_{uv} = 12 min exhibited the highest mobility of 4.76 $cm^2\ V^{-1}\ s^{-1}$. The μ_{sat} value is reasonable for C_8-BTBT OTFTs fabricated by spin-coating with bottom-gate-top-contact structure.[17, 39–41] The short and long irradiation times led to low mobility, as seen in Fig. 5(a).

5. Discussion

The effect of the second UV irradiation is discussed in this section. The modification of an alkyl-monolayer by VUV has been reported.[31–33] The methyl-terminated groups are converted to hydrophilic oxygenated carbon components by a photochemical reaction. In the research studies, VUV with the intensity of about 10 mW/cm^2 was applied to the monolayers, similar to that used in this study. Therefore, the results in the earlier studies support the discussion of our results. Figure 6 shows the XPS spectra of the C(1s) region for substrates with a trimethylsilyl-monolayer unirradiated and irradiated with VUV for t_{uv} = 15 min. The spectra have a strong peak at 284.4 eV, possibly relating to carbon atoms in methyl groups and hydrocarbon contamination on the substrate. For the substrate irradiated with VUV, a peak appeared at 288.7 eV. In addition, the intensity around 285.9 eV increased. Similar spectra have been observed in the studies for a VUV-irradiated alkyl-monolayer.[31, 42] The deconvoluted spectra are indicated in the image by the colored solid lines. The week peaks at 288.1 and 285.9 eV are possibly assigned to the binding energies of the oxygenated groups of $-COOH$ and $-CH_2OH$, respectively,[31, 33, 42] suggesting that the formation of oxygenated groups affected the characteristic of the OTFTs.

For the transistor characteristics, the transfer curve in the reverse sweep shifted to negative gate voltage as compared to that in the forward sweep, as seen in Fig. 4. The shift is explained by the increase in the charge on the gate dielectric surface. The increase is attributed to trapping holes

at sites [5)] and/or releasing electrons captured at sites on the gate dielectric surface. The number of charges trapped per unit (N_{trap}) is estimated as $N_{trap} = |\Delta V_{th}| C_{ox}/e$ where e is elementary charge.[43)] For Fig. 4(a), N_{trap} for the OTFTs without monolayer is calculated as 1.3×10^{12} cm^{-2}. The N_{trap} value is close to that for a hydrophilic SiO_2/Si substrate without monolayer treated by oxygen plasma.[44)] From the comparison, the hysteresis observed for the OTFT without monolayer may be due to the formation of ≡SiOH groups on the gate dielectric surface by the first VUV irradiation. The detailed mechanism of the hysteresis associated with the ≡SiOH groups has been examined,[5, 44)] indicating that the molecules adsorbed on the dielectric surface, especially water, cause hysteresis.[43, 45–47)] In that case, the orbital of the adsorbed molecules creates the trap levels.[47, 48)] Dipolar molecules in ambient conditions are easily adsorbed on the hydrophilic polar ≡SiOH groups on a dielectric surface, resulting in an increase in the hysterics. Furthermore, the trimethylsilyl-monolayer reduced the dependence of the hysteresis in ambient conditions.[44)]

The hydrophilic polar −COOH and $-CH_2OH$ groups generated by the second UV irradiation may degrade the performance of OTFTs in the same mechanism. The optimal second UV irradiation for 12 min generated the oxygenated carbon components, providing a hydrophilic surface and possibly leaving a considerable amount of nonpolar $-CH_3$ groups. Therefore, OTFTs fabricated under the condition exhibited a high mobility and low hysteresis. Then, excessive VUV irradiation increased the total percentage of polar groups of a monolayer, including the ≡SiOH groups. Although the μ_{sat} value for t_{uv} = 60 min was close to that of an OTFT without the monolayer, the ΔV_{th} value for t_{uv} = 60 min was quite different from that of an OTFT without monolayer. This suggests that the surface obtained by VUV irradiation on an SiO_2 gate dielectric covered with a trimethylsilyl-monolayer for long time differed from that without a monolayer. HMDS treatment additionally provided Si atoms to the SiO_2 surface. Although VUV irradiation dissociate $-CH_3$

groups in a trimethylsilyl-monolayer and the product evaporated, Si atoms in the monolayer probably remained on the surface. This is because Si-O bond was strong and the vapor pressure of a product, including Si was low. The additional Si atoms may cause a difference between the surfaces mentioned above. A part of the Si atoms was oxidized by the active oxygen species.[31] Therefore, the large difference in ΔV_{th} possibly attributed to the surface changes.

From above discussion, the adjustment of VUV irradiation time was important to achieve the high-performance OTFTs. The μ_{sat} value for t_{uv} = 10 min was less than that for 12 min. Probably, the properties of a C_8-BTBT film related to the difference in μ_{sat}. The slightly low μ_{sat} for t_{uv} = 10 min may be due to the non-uniformity and/or low adhesion of the organic thin-film. The partial film formation seen in Fig. 2(c) seems to be associated with the lack of uniformity and low adhesion. The coverage for t_{uv} = 10 min was similar to that for t_{uv} = 12 min, as seen in Fig. 2(c). Thus, the large error bar in Figs. 5(a) and (b) might be of the same origin. There is no large difference in the crystallinity in the resolution of the optical microscope for t_{uv} = 10 and 12 min.

6. Conclusions

We investigated the effect of the VUV light irradiation on the gate dielectric surface covered with a trimethylsilyl-monolayer and characteristics of C_8-BTBT based OTFTs. The irradiation gradually changes the hydrophobic surface covered with a trimethylsilyl-monolayer into a hydrophilic surface, explained by an increase in the surface free energy. As a result, the irradiation to a monolayer enables the formation of an organic film by solution-process. The XPS measurement indicates that the irradiation of VUV to a hydrophobic trimethylsilyl-monolayer oxidizes the $-CH_3$ groups and generates hydrophilic $-CH_2OH$ and $-COOH$ groups by photochemical reaction. The result of the OTFT measurement suggests that there is an optimal irradiation time. This is because excessive irradiation leads to a decrease in the mobility and large

hysteresis in the transfer curve. The degradation of the transistor characteristics implies an increase in trap sites by VUV irradiation. The OTFTs with a C_8-BTBT film deposited on the optimal hydrophilic substrate by spin-coating showed the average mobility of 4.1 $cm^2 V^{-1} s^{-1}$ and exhibited the highest mobility of 4.76 $cm^2 V^{-1} s^{-1}$. A monolayer partially modified by conventional UV/O_3 treatment is applicable for a variety of solution-processes for organic semiconductors toward prospective printed electronics.

ACKNWLEDGEMENTS

This work was partly supported by a Leading Initiative for Excellent Young Researchers program from the MEXT in Japan, JSPS KAKENHI Grant Numbers 19H02171, 21K04195, 21H04655, and Kansai Research Foundation. The authors also thank Nippon Kayaku Co., Ltd. for supplying us C_8-BTBT.

REFERENCES

1) H. Iino, T. Usui and J. Hanna, Nat Commun **6**, 6828 (2015).

2) Z. Zhang, B. Peng, X. Ji, K. Pei and P. K. L. Chan, Advanced Functional Materials **27**, 1703443 (2017).

3) T. Uemura, K. Nakayama, Y. Hirose, J. Soeda, M. Uno, W. Li, M. Yamagishi, Y. Okada and J. Takeya, Current Applied Physics **12**, S87 (2012).

4) R. Ruiz, A. Papadimitratos, A. C. Mayer and G. G. Malliaras, Advanced Materials **17**, 1795 (2005).

5) M. Egginger, S. Bauer, R. Schwödiauer, H. Neugebauer and N. S. Sariciftci, Monatsh Chem **140**, 735 (2009).

6) S. H. Kim, H. Yang, S. Y. Yang, K. Hong, D. Choi, C. Yang, D. S. Chung and C. E. Park, Organic Electronics **9**, 673 (2008).

7) S. C. Lim, S. H. Kim, J. H. Lee, M. K. Kim, D. J. Kim and T. Zyung, Synthetic Metals **148**, 75 (2005).

8) T. Umeda, D. Kumaki and S. Tokito, Journal of Applied Physics **105**, 024516 (2009).

9) T. Yasuda, K. Fujita, H. Nakashima and T. Tsutsui, Jpn. J. Appl. Phys. **42**, 6614 (2003).

10) W. L. Kalb, T. Mathis, S. Haas, A. F. Stassen and B. Batlogg, Appl. Phys. Lett. **90**, 092104 (2007).

11) D. Knipp, R. A. Street, A. Völkel and J. Ho, Journal of Applied Physics **93**, 347 (2003).

12) M. Shtein, J. Mapel, J. B. Benziger and S. R. Forrest, Appl. Phys. Lett. **81**, 268 (2002).

13) J. B. Koo, S. H. Kim, J. H. Lee, C. H. Ku, S. C. Lim and T. Zyung, Synthetic Metals **156**, 99 (2006).

14) J. Roh, C. Kang, J. Kwak, C. Lee and B. Jun Jung, Appl. Phys. Lett. **104**, 173301 (2014).

15) K. Kuribara, H. Wang, N. Uchiyama, K. Fukuda, T. Yokota, U. Zschieschang, C. Jaye, D. Fischer, H. Klauk, T. Yamamoto, K. Takimiya, M. Ikeda, H. Kuwabara, T. Sekitani, Y.-L. Loo and T. Someya, Nat Commun **3**, 723 (2012).

16) K. Fukuda, T. Hamamoto, T. Yokota, T. Sekitani, U. Zschieschang, H. Klauk and T. Someya, Appl. Phys. Lett. **95**, 203301 (2009).

17) F. Dai, X. Liu, T. Yang, J. Qian, Y. Li, Y. Gao, P. Xiong, H. Ou, J. Wu, M. Kanehara, T. Minari and C. Liu, ACS Appl. Mater. Interfaces **11**, 7226 (2019).

18) Z. Chai, S. A. Abbasi and A. A. Busnaina, ACS Appl. Mater. Interfaces **10**, 18123 (2018).

19) J. Tsurumi, A. Y. Amin, T. Okamoto, C. Mitsui, K. Takimiya, H. Matsui, M. Halik and J. Takeya, Organic Electronics **15**, 1184 (2014).

20) H.-R. Tseng, H. Phan, C. Luo, M. Wang, L. A. Perez, S. N. Patel, L. Ying, E. J. Kramer, T.-Q. Nguyen, G. C. Bazan and A. J. Heeger, Advanced Materials **26**, 2993 (2014).

21) H. Minemawari, T. Yamada, H. Matsui, J. Tsutsumi, S. Haas, R. Chiba, R. Kumai and T. Hasegawa, Nature **475**, 364 (2011).

22) W. Kang, M. Kitamura and Y. Arakawa, Appl. Phys. Express **4**, 121602 (2011).

23) H. Zhao, D. Li, G. Dong, L. Duan, X. Liu and L. Wang, Langmuir **30**, 12082 (2014).

24) N. Herzer, S. Hoeppener and U. S. Schubert, Chemical Communications **46**, 5634 (2010).

25) T. Schmaltz, G. Sforazzini, T. Reichert and H. Frauenrath, Advanced Materials **29**, 1605286 (2017).

26) Y.-H. Kim, B. Yoo, J. E. Anthony and S. K. Park, Advanced Materials **24**, 497 (2012).

27) K. Bulgarevich, K. Sakamoto, T. Minari, T. Yasuda and K. Miki, ACS Appl. Mater. Interfaces **9**, 6237 (2017).

28) G. Giri, E. Miller and Z. Bao, Journal of Materials Research **29**, 2615 (2014).

29) M. Kano, T. Minari and K. Tsukagoshi, Appl. Phys. Express **3**, 051601 (2010).

30) K. Kuribara, T. Nobeshima, A. Takei, T. Kodzasa, S. Uemura and M. Yoshida, Jpn. J. Appl. Phys. **58**, 041002 (2019).

31) A. I. A. Soliman, T. Ichii, T. Utsunomiya and H. Sugimura, Soft Matter **11**, 5678 (2015).

32) T. Ye, E. A. McArthur and E. Borguet, J. Phys. Chem. B **109**, 9927 (2005).

33) L. Hong, H. Sugimura, T. Furukawa and O. Takai, Langmuir **19**, 1966 (2003).

34) T. Ye, D. Wynn, R. Dudek and E. Borguet, Langmuir **17**, 4497 (2001).

35) H. Sugimura, K. Ushiyama, A. Hozumi and O. Takai, Langmuir **16**, 885 (2000).

36) P. Prisawong, P. Zalar, A. Reuveny, N. Matsuhisa, W. Lee, T. Yokota and T. Someya, Advanced Materials **28**, 2049 (2016).

37) S. Inoue, Y. Hattori and M. Kitamura, Ext. Abstr. 11 th Int. Conf. Flexible and Printed Electronics, 2020, 01-19-06.

38) Y. Hattori and M. Kitamura, ACS Appl. Mater. Interfaces **12**, 36428 (2020).

39) T. Shen, H. Zhou, X. Liu, Y. Fan, D. D. Mishra, Q. Fan, Z. Yang, X. Wang, M. Zhang and J. Li, ACS Omega **5**, 10891 (2020).

40) A. Pérez-Rodríguez, I. Temiño, C. Ocal, M. Mas-Torrent and E. Barrena, ACS Appl. Mater. Interfaces **10**, 7296 (2018).

41) Y. Li, C. Liu, Y. Xu, T. Minari, P. Darmawan and K. Tsukagoshi, Organic Electronics **13**, 815 (2012).

42) S. L. Brandow, M.-S. Chen, R. Aggarwal, C. S. Dulcey, J. M. Calvert and W. J. Dressick, Langmuir **15**, 5429 (1999).

43) C.-J. Shih, G. L. C. Paulus, Q. H. Wang, Z. Jin, D. Blankschtein and M. S. Strano, Langmuir **28**, 8579 (2012).

44) M. Lafkioti, B. Krauss, T. Lohmann, U. Zschieschang, H. Klauk, K. v. Klitzing and J. H. Smet, Nano Lett. **10**, 1149 (2010).

45) A. Veligura, P. J. Zomer, I. J. Vera-Marun, C. Józsa, P. I. Gordiichuk and B. J. van Wees, Journal of Applied Physics **110**, 113708 (2011).

46) T. Lohmann, K. von Klitzing and J. H. Smet, Nano Lett. **9**, 1973 (2009).

47) O. Leenaerts, B. Partoens and F. M. Peeters, Phys. Rev. B **77**, 125416 (2008).

48) Z.-M. Liao, B.-H. Han, Y.-B. Zhou and D.-P. Yu, J. Chem. Phys. **133**, 044703 (2010).

FIGURE CAPTIONS

Figure 1: **(a)–(f)** Fabrication process of an OTFT with a trimethylsilyl-monolayer irradiated with UV light: **(a)** First UV irradiation for 30 min, **(b)** Formation of a trimethylsilyl-monolayer from HMDS vapor, **(c)** Second UV irradiation for t_{uv}, **(d)** Formation of a C_8-BTBT layer by spin-coating, **(e)** Deposition of electrodes, **(f)** Isolation of an OTFT using a fine needle, **(g)** Photograph of the fabricated OTFT.

Figure 2: **(a)** Setup of UV light irradiation and distribution of the UV light intensity, **(b)** Water contact angles on an SiO_2 surface covered with a trimethylsilyl-monolayer irradiated for t_{uv}, **(c)** Photographs of an organic thin-film deposited by spin-coating for the different second UV irradiation time.

Figure 3: Optical microscope images of the organic thin-film for the substrate with the second UV irradiation for 10 min. **(a)** Bright-field microscopy image, **(b) and (c)** Polarized light microscopy images. The angle between the two transmission axes is intentionally rotated by about 5° from 90° to enhance the contrast.

Figure 4: Transfer curves in the saturation regime for the substrates **(a)** Without monolayer, and with an HMDS-treated monolayer irradiated with VUV for **(b)** 12 min and **(c)** 60 min, **(d)** Output characteristics of an OTFT with a monolayer VUV-irradiated for t_{uv} = 12 min.

Figure 5: **(a)** μ_{sat} and **(b)** ΔV_{th} as functions of the second UV irradiation time.

Figure 6: XPS of the C(1s) region for the HMDS-treated substrate **(a)** without and **(b)** with the second UV irradiation.

Table 1 Electrical properties of typical OTFTs for different UV irradiation time.

t_{uv} (min)	μ_{sat} ($cm^2\ V^{-1}\ s^{-1}$)	V_{thf} (V)	V_{thr} (V)	ΔV_{th} (V)	ON/OFF ratio (−)
w/o monolayer	1.64	−8.53	−14.9	−6.36	1.88×10^7
10	3.15	−6.70	−8.55	−1.85	4.66×10^6
12	4.76	−8.58	−9.13	−0.55	4.31×10^6
15	4.41	−6.68	−8.11	−1.43	1.07×10^6
20	3.55	−7.39	−9.27	−1.88	2.00×10^6
30	3.24	−7.94	−10.0	−2.06	2.20×10^6
60	1.90	−7.91	−10.8	−2.89	7.76×10^6

FIGURES

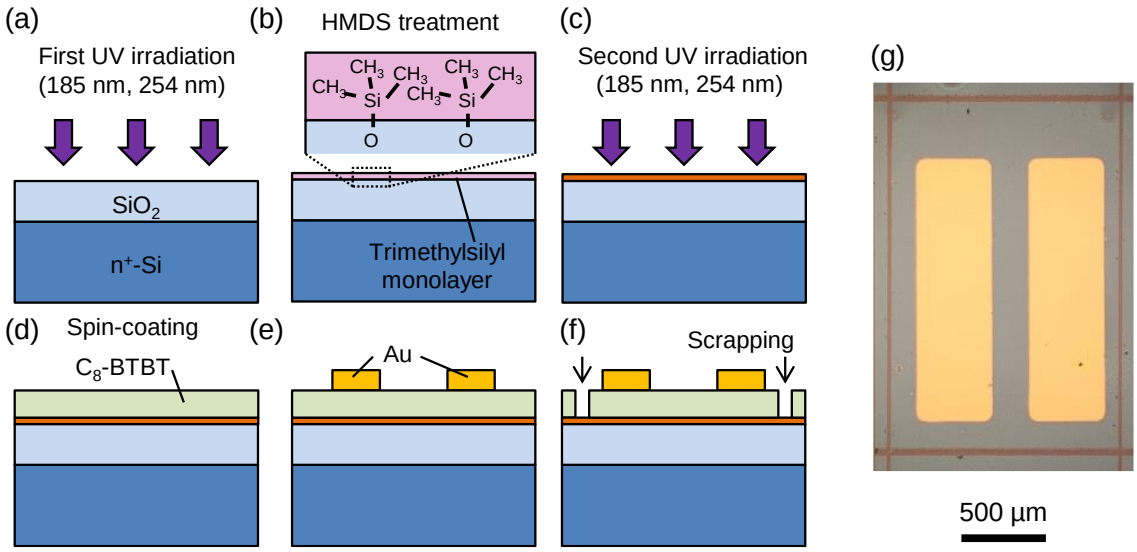

Figure 1: **(a)–(f)** Fabrication process of an OTFT with a trimethylsilyl-monolayer irradiated with UV light: **(a)** First UV irradiation for 30 min, **(b)** Formation of a trimethylsilyl-monolayer from HMDS vapor, **(c)** Second UV irradiation for t_{uv}, **(d)** Formation of a C_8-BTBT layer by spin-coating, **(e)** Deposition of electrodes, **(f)** Isolation of an OTFT using a fine needle, **(g)** Photograph of the fabricated OTFT.

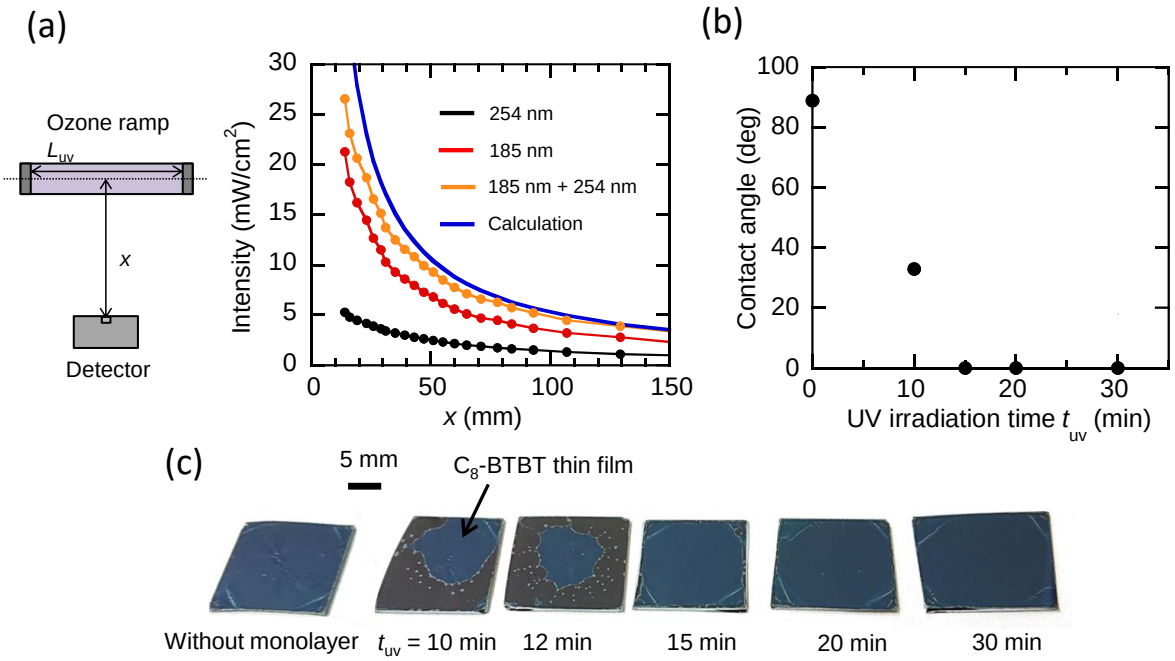

Figure 2: **(a)** Setup of UV light irradiation and distribution of the UV light intensity, **(b)** Water contact angles on an SiO_2 surface covered with a trimethylsilyl-monolayer irradiated for t_{uv}, **(c)** Photographs of an organic thin-film deposited by spin-coating for the different second UV irradiation time.

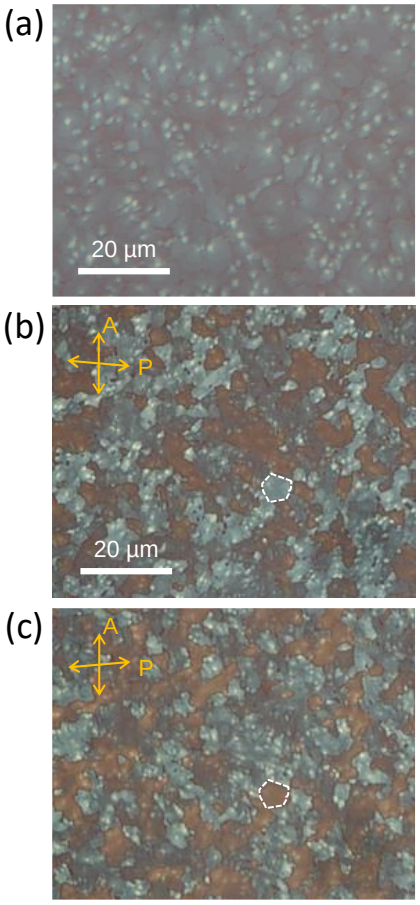

Figure 3: Optical microscope images of the organic thin-film for the substrate with the second UV irradiation for 10 min. **(a)** Bright-field microscopy image, **(b) and (c)** Polarized light microscopy images. The angle between the two transmission axes is intentionally rotated by about 5° from 90° to enhance the contrast.

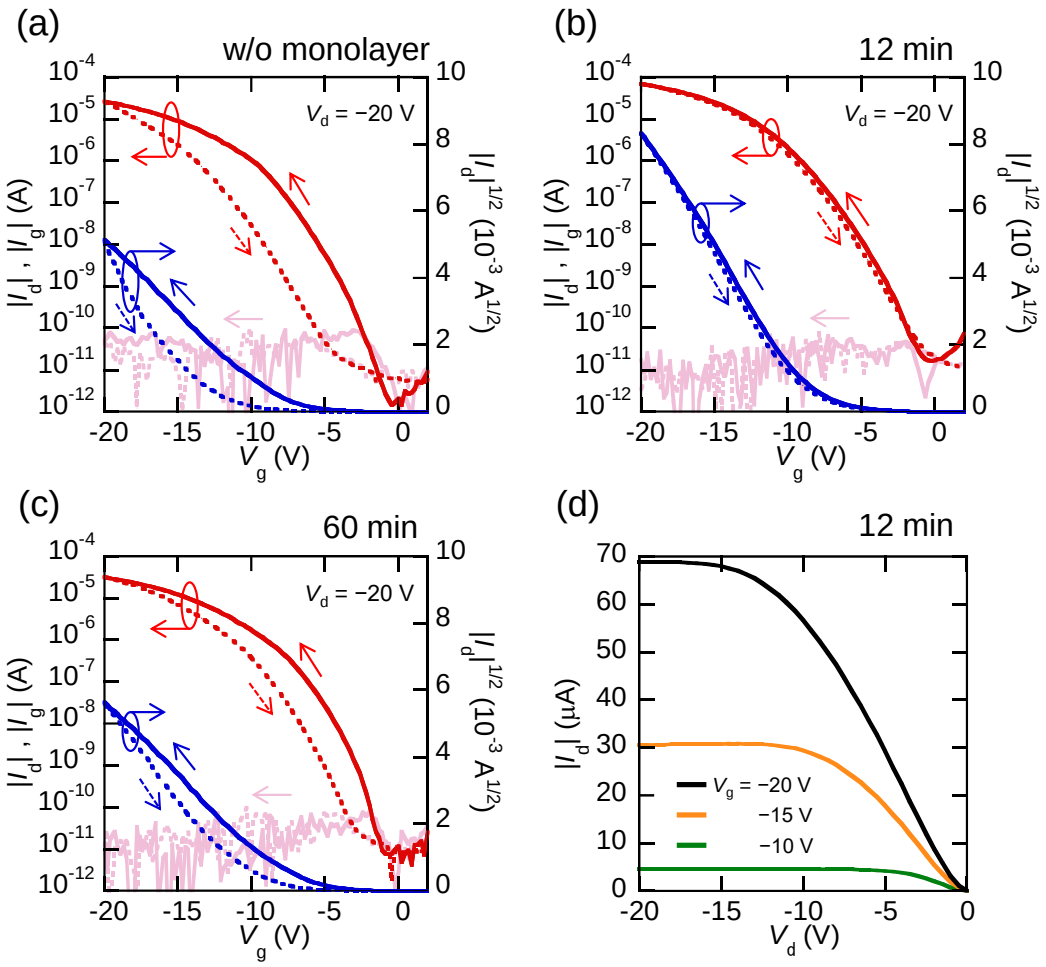

Figure 4: Transfer curves in the saturation regime for the substrates **(a)** Without monolayer, and with an HMDS-treated monolayer irradiated with VUV for **(b)** 12 min and **(c)** 60 min, **(d)** Output characteristics of an OTFT with a monolayer VUV-irradiated for t_{uv} = 12 min.

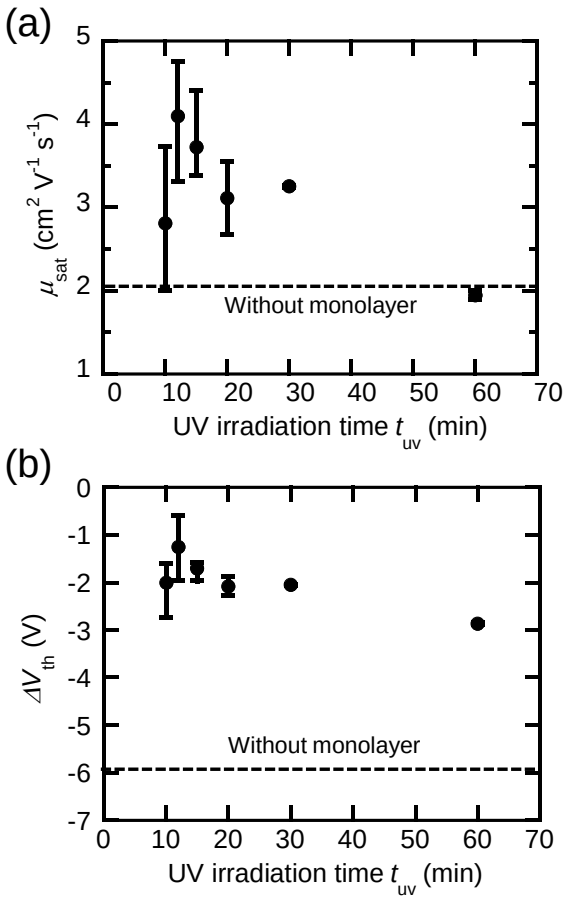

Figure 5: **(a)** μ_{sat} and **(b)** ΔV_{th} as functions of the second UV irradiation time.

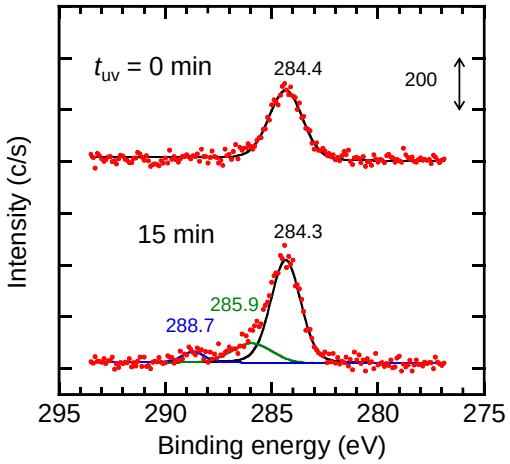

Figure 6: XPS of the C(1s) region for the HMDS-treated substrate **(a)** without and **(b)** with the second UV irradiation.